 doi:10.20944/preprints202102.0031.v1

Article

Investigating primary cilia during peripheral nervous system formation

Elkhan Yusifov [1], Alexandre Dumoulin [1] and Esther T. Stoeckli [1,*]

[1] Department of Molecular Life Sciences and Neuroscience Center Zurich, University of Zurich, Winterthurerstrasse 190, 8057 Zurich, Switzerland; elkhan.yusifov@uzh.ch (E.Y); alexandre.dumoulin@mls.uzh.ch (A.D.)

* Correspondence: esther.stoeckli@mls.uzh.ch; Tel.: +41 44 635 4840

Abstract: The primary cilium plays a pivotal role during embryonic development of vertebrates. It acts as a somatic signaling hub for specific pathways, such as sonic hedgehog signaling. In humans, mutations in genes that cause dysregulation of ciliogenesis or ciliary function lead to severe developmental disorders called ciliopathies. Beyond its obvious role in early morphogenesis, growing evidence points towards an essential function of the primary cilium in neural circuit formation in the central nervous system. However, very little is known about a potential role in the formation of the peripheral nervous system. Here, we investigated the presence of the primary cilium in neural crest cells and their derivatives in the trunk of the developing chicken embryo in vivo. We found that neural crest cells, sensory neurons, and boundary cap cells all bear a primary cilium during key stages of early peripheral nervous system formation. Moreover, we described differences in the ciliation of neuronal cultures of different populations from the peripheral and central nervous system. Our results offer a framework for further in vivo and in vitro investigations on specific roles that the primary cilium might play during peripheral nervous system formation.

Keywords: primary cilium, ciliogenesis, neural circuits formation, neural crest cells, DRG, boundary cap cells, sympathetic ganglia, PNS

1. Introduction

The primary cilium is a tiny non-motile organelle that can be seen on most vertebrate cells [1–3]. It was discovered by the Swiss neuroscientist Zimmermann in 1898 [4]. After its discovery, the primary cilium was neglected for a century as an evolutionary rudiment. However, studies in the last two decades have characterized the primary cilium as a signaling hub involved in distinct signaling cascades, such as Sonic Hedgehog (Shh)[5,6], Wnt [7,8], PDGFR [9,10], mTOR [11], and other pathways. Subsequent studies demonstrated that the primary cilium is involved in differentiation, proliferation, survival, polarity, and migration of cells [12]. That is why defects in the genes responsible for cilium formation and function have been identified as cause for a group of disorders gathered under the umbrella of ciliopathies [13,14]. Common features in ciliopathies include retinal degeneration, craniofacial defects, polydactyly, intellectual disability, situs inversus, and cystic kidneys. As suggested by the name, proteins involved in ciliopathies are located either inside or at the base of primary cilia [15]. Mutations in genes responsible for primary cilia formation cause defective ciliary function in non-motile ciliopathies, and thus, trigger various developmental and degenerative phenotypes in different tissues such as the kidney, the retina and the brain [16,17]. Human patients with ciliopathies, such as Joubert syndrome, can show pronounced abnormalities in the formation of the central nervous system (CNS). Translating observations from humans into model organisms helped to characterize pathological processes related to the loss of functional primary cilia at different levels, such as neuronal differentiation, migration, and axon tract formation [18–20]. However, to date, the potential role that the primary cilium might play during the formation of the peripheral nervous system is still poorly characterized, although several studies suggested such a role [21,22].

 doi:10.20944/preprints202102.0031.v1

Neural crest cells (NCC) of the trunk are multipotent cells that delaminate from the dorsal neural tube and migrate laterally and ventrally using distinct trajectories. When they reach their final destination, they differentiate into dorsal root ganglia (DRG) neurons, sympathetic ganglia (SG) neurons, boundary cap cells (BCC), or glial cells [23,24]. Neural crest cell development is therefore a prerequisite in the formation of a fully functional PNS. Each step in the development of NCC, delamination, migration and differentiation into their derivatives, is temporally and transcriptionally regulated [25].

To learn more about a possible role of primary cilia in PNS development, it was crucial to investigate first whether distinct NCC populations possessed a primary cilium during key stages of development *in vivo*. We could assess and confirm the presence of a primary cilium in migrating NCC and their derivatives, such as DRG neurons, SG neurons, and BCC *in vivo.* This confirmed that the primary cilium might be engaged in the development of the PNS at multiple levels. Moreover, we also characterized the timing of ciliation in dissociated and explant cultures of PNS and CNS neurons. We found that dissociated DRG neurons did not recover their primary cilium, whereas other neuronal populations, such as commissural neurons and motoneurons, largely did, albeit with distinct timing. Furthermore, when cultured as explants, neurons did not lose primary cilia in culture. Taken together, these findings will be useful for scientists trying to decipher molecular mechanisms of PNS assembly and the primary cilium *in vivo* and *in vitro*.

2. Results

2.1. Trunk neural crest cells bear a primary cilium during their early migration

NCC delaminating from the lumbar neural tube start migrating in a dorsal-to-ventral direction around Hamburger and Hamilton stage 16 (HH16) in the chicken embryo and will then settle in their final destination prior to differentiation (Figure 1A-C) [26,27]. Immunohistochemistry was used to visualize the migration of NCC and to characterize whether NCC possessed a primary cilium during their migration and early settlement *in vivo*. We stained transverse spinal cord cryosections for the NCC marker HNK1 [27] and for the primary cilium marker Arl13B (

Figure **1**D) [28]. These multipotent stem cells bore a primary cilium during their early migration before arriving at the dorsal roots level (white arrows,

Figure **1**E,F). Migrating NCC reached the ventral roots at HH17 (

Figure **1**B,G) and the area lateral of the notochord at HH18 (

Figure **1**C,I). During migration and settlement, we found primary cilia located on the soma of NCC (white arrows,

Figure **1**H,J).

Taken together, our data revealed that just after undergoing epithelial-to-mesenchymal transition and delamination, NCC already bore a primary cilium and maintained it during their migration and early settlement.

Preprints (www.preprints.org) | NOT PEER-REVIEWED | Posted: 1 February 2021 doi:10.20944/preprints202102.0031.v1

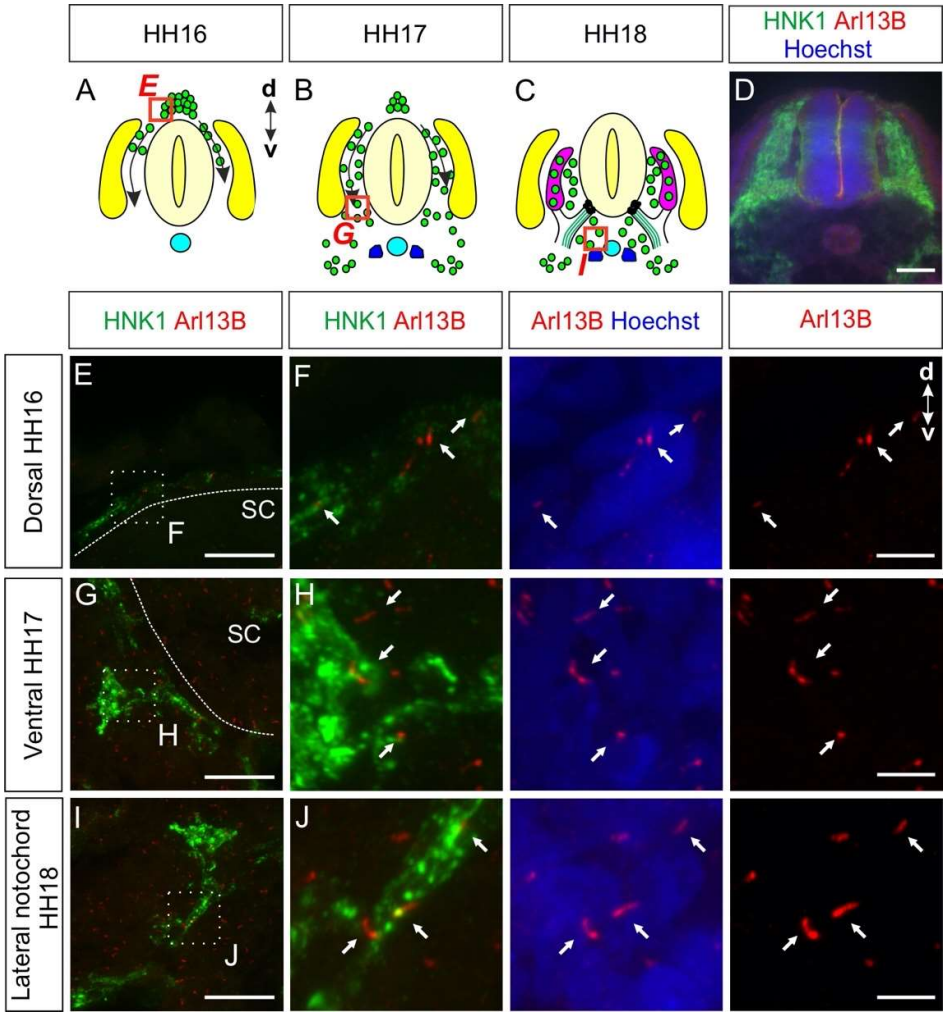

Figure 1. Trunk neural crest cells (NCC) possessed a primary cilium during early migration and settlement. **(A-C)** Trunk NCC migrate ventrally between HH16 and HH18 on both sides of the neural tube. Green: NCC, turquoise: notochord, purple: DRG, yellow: dermomyotome, blue: sympathetic ganglia chain, black dots: BCC, green lines: ventral roots. d, dorsal; v, ventral. **(D)** A transverse section of the spinal cord of a HH18 embryo stained with HNK1 to stain NCC (green) and with Arl13B antibodies to visualize primary cilia (red). Nuclei were counterstained with Hoechst (blue). **(E,F)** NCC were visualized at HH16 before arriving at the dorsal root level. They were found to bear a primary cilium (white arrows). **(G-J)** NCC located at the ventral root level **(G)** and the area lateral to the notochord **(I)** possessed a primary cilium (white arrows). Squares with dashed lines represent the region of interest shown in right panels. Dashed lines represent the boundary of the spinal cord. d, dorsal; v, ventral; SC, spinal cord. Scale bars: 100 μm (D), 25 μm (E,G,I) and 5 μm (F,H,J).

2.2. Dorsal root ganglia neurons carry a primary cilium during development

We then asked whether the primary cilium was maintained in NCC derivatives during development. We first focused on the sensory neurons located in the DRG. We found that the first Islet-1-positive, differentiated DRG neurons carried a primary cilium at HH18 (white arrows, Figure 2A). Interestingly, Islet-1-negative cells in the DRG also had a primary cilium suggesting that either neuronal or Schwann cell precursors were ciliated (open arrow, Figure 2A). Later on, the same observation was made in DRG neurons at HH26 and HH30 with cilia evenly distributed throughout the DRG (white arrows, Figure 2B,C). We found that 86 ± 5% of Hoechst-positive cells carried a primary cilium in HH26 DRG. Given the fact that 75 ± 3% of these cells were Islet-1-positive (mean ± standard deviation, N(embryos) = 3, n(DRG) = 12), this suggested that the large majority of DRG neurons were ciliated at this stage. In line with these results, we made similar observations in the

Preprints (www.preprints.org) | NOT PEER-REVIEWED | Posted: 1 February 2021 doi:10.20944/preprints202102.0031.v1

mouse at embryonic day E11.5, at the time, when DRG afferents enter the spinal cord (white arrows, Figure 2D) [29]. We also obtained the same results with alternative approaches in HH26 chicken embryos. We could co-stain DRG neurons with the intraflagellar transport protein IFT88 (arrows, Supplementary Figure 1) [30]. Furthermore, we utilized *in ovo* electroporation to transfect Arl13B-RFP in NCC and their derivatives, and could reveal the presence of primary cilia in Islet-1-positive DRG neurons (white arrow, Figure 2E).

Altogether, these results showed that DRG neurons maintained their primary cilium when they polarize, send their axons towards the periphery and the CNS, and connect to the deeper layers of the spinal cord [31].

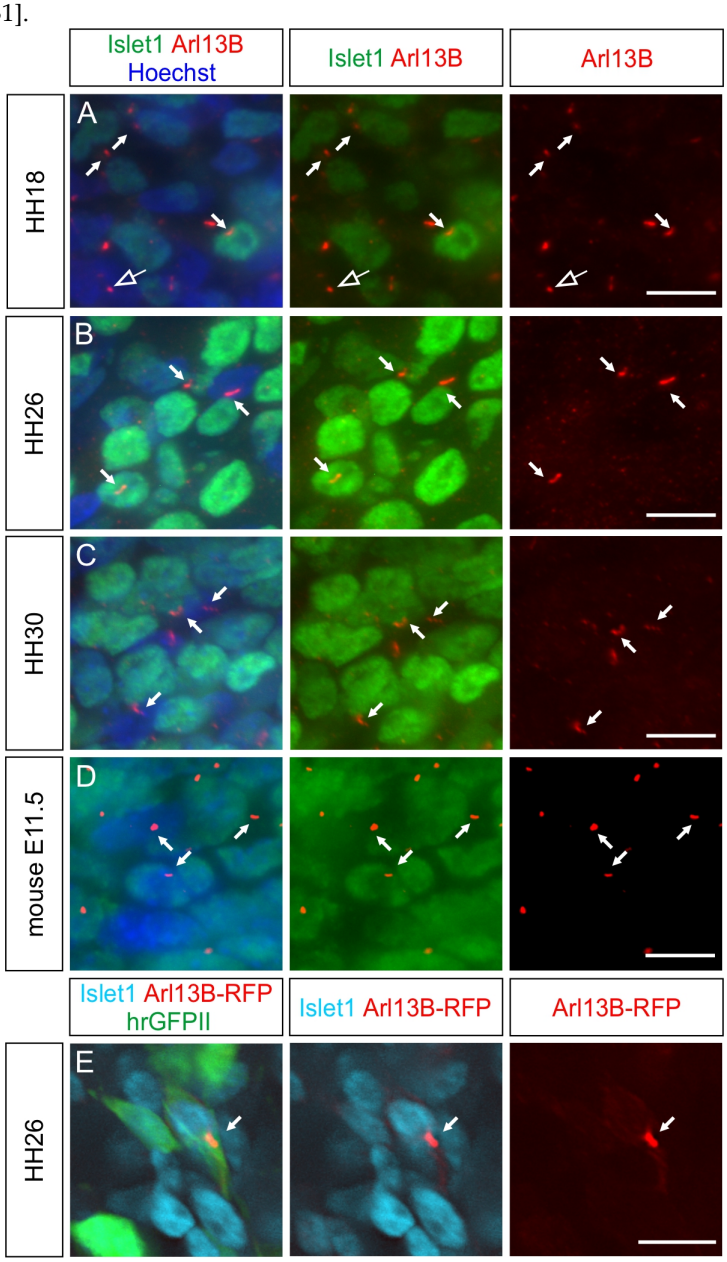

Figure 2. Embryonic DRG neurons possessed a primary cilium in chicken and mouse embryos. **(A-D)** Micrographs of Islet1-positive DRG neurons (green) bearing an Arl13B-positive primary cilium (red, white arrows) at stage HH18, HH26, and HH30. The open arrow points to a primary cilium on an Islet-1-negative cell. **(D)** E11.5 mouse DRG neurons also possessed a primary cilium (white arrows). Nuclei were counterstained with Hoechst (blue). (E) Primary cilia were visible after RFP staining (red) of HH26 Islet-1-positive DRG neurons (cyan) after co-electroporation of Arl13B-RFP (white arrow) with hrGFPII (green). Dorsal is up. Scale bars: 10 μm (A-D) and 5 μm (E).

 doi:10.20944/preprints202102.0031.v1

2.3. Boundary cap cells bear a primary cilium at both ventral and dorsal roots

During the assembly of the chicken trunk PNS, a subtype of migrating NCC will first stop and cluster at the ventral roots exit points (also termed motor axon exit points) of the spinal cord around HH18, as revealed by 1E8 immunostaining, recognizing the P0 protein (white open arrowheads, Figure3A). Later, other NCC will do the same at the dorsal root entry zone level (white arrowheads, Figure3A). These cells are the boundary cap cells (BCC) and are located at the interface between the CNS and the PNS. They play a role as gatekeepers between the CNS and PNS and they represent stem cells that later contribute to subtypes of sensory neurons, glial cells, and pericytes [32,33]. Using co-immunostaining of the BCC marker 1E8 and the primary cilium marker Arl13B, we were able to see that ventral and dorsal BCC bore a primary cilium at all stages investigated *in vivo* (HH18-HH30, white arrows, Figure 3B-E and Supplementary Figure 2).

Overall, our results indicated that BCC bear a primary cilium throughout early stages of development, when neural circuits in the PNS and CNS are formed.

Preprints (www.preprints.org) | NOT PEER-REVIEWED | Posted: 1 February 2021 doi:10.20944/preprints202102.0031.v1

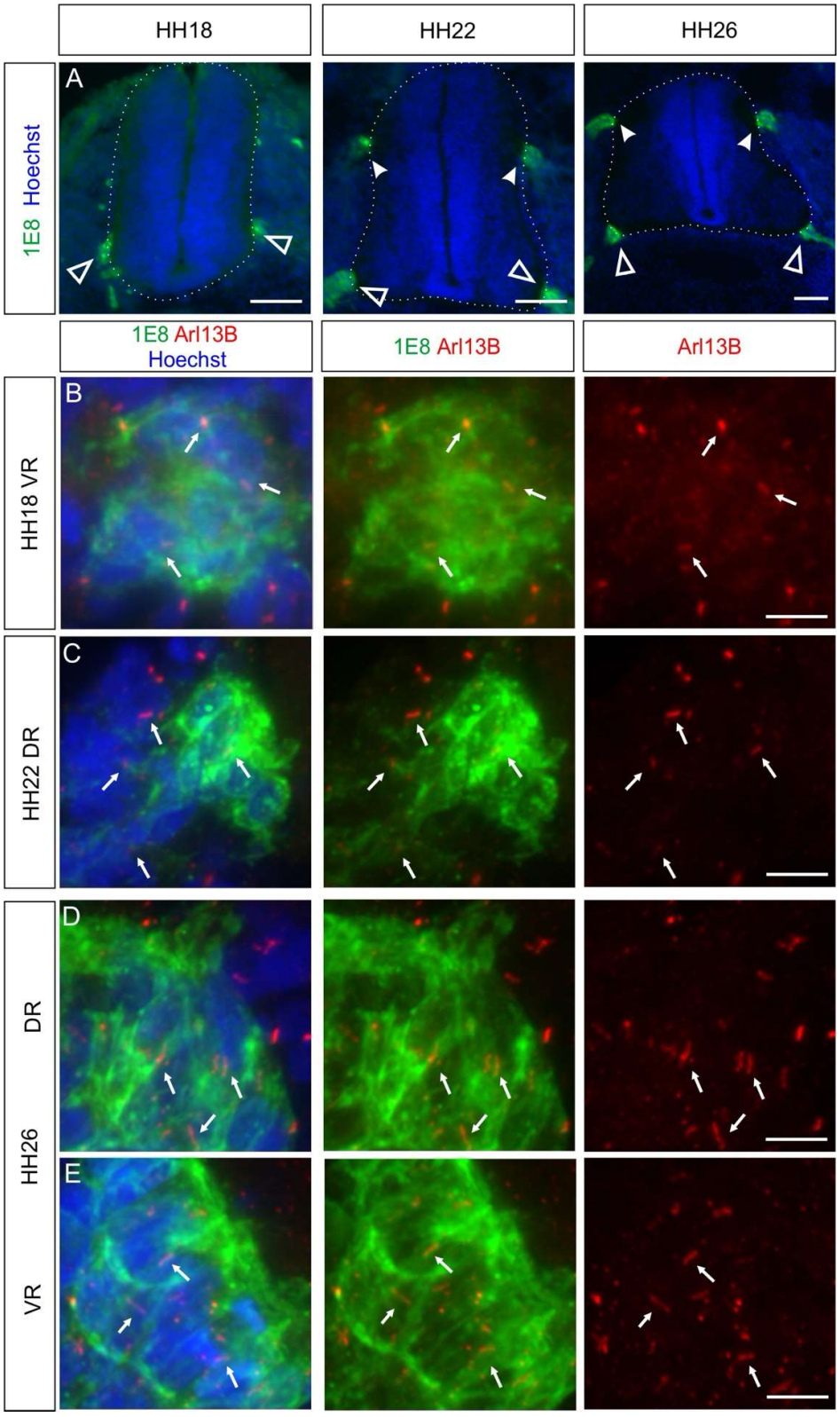

Figure 3. BCC possessed a primary cilium during early development of the CNS-PNS boundary. BCC were stained with 1E8 antibodies (green) and primary cilia with Arl13B antibodies (red). **(A)** BCC clusters were initially detected at the ventral roots at HH18 (white open arrowheads). BCC clusters at the dorsal roots were observed at HH22 (white arrowheads). Nuclei were counterstained with Hoechst (blue). **(B-E)** BCC were ciliated

Preprints (www.preprints.org) | NOT PEER-REVIEWED | Posted: 1 February 2021 doi:10.20944/preprints202102.0031.v1

both at dorsal and ventral roots between HH18 and HH26 (white arrows). White dashed lines represent the boundary of the spinal cord (CNS). DR, dorsal roots; VR, ventral roots. Dorsal is up. Scale bars: 100 μm (A) and 10 μm (B-E).

2.4. Carrying a primary cilium appears to be a common feature on NCC derivatives in vivo

To further complement our *in vivo* characterization of ciliation, we also assessed two other populations of NCC derivatives: the sympathetic ganglia (SG) neurons and the melanocytes.
SG neurons are located in the SG chains and are part of the autonomic nervous system [34]. Co-immunostaining of the SG neurons markers Islet-1 or Tyrosine hydroxylase (TH) together with the primary cilia marker Arl13B revealed that these neurons were ciliated at HH26 (white arrows, Figure 4A,B).
A subset of trunk NCC after delamination will migrate dorso-laterally and constitute the melanocyte lineage to form ultimately melanocytes in the skin [23,26]. We visualized melanocytes in the skin of the trunk at HH26 using the MelEM antibody and could see that these cells bore a primary cilium with Arl13B co-staining (white arrows, Supplementary Figure 3).
Collectively, our results showed that both SG neurons during their early development and melanocytes located in the skin bore a primary cilium.

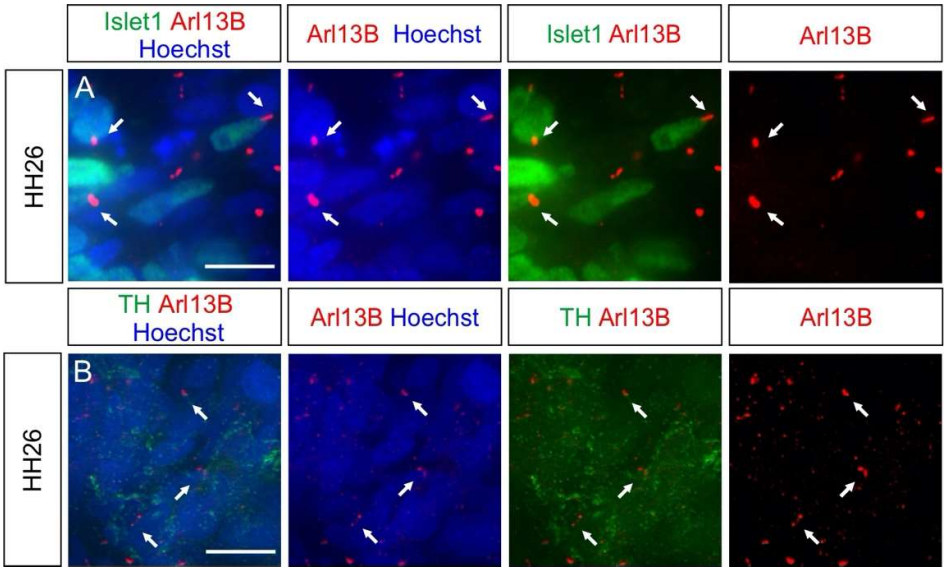

Figure 4. Other NCC derivatives such as sympathetic ganglia (SG) neurons possessed a primary cilium. Islet-1 **(A)** and TH **(B)** antibodies were used to stain HH26 SG neurons (green). **(A,B)** Arl13B staining revealed that these neurons were ciliated (white arrows). Nuclei were counterstained with Hoechst (blue). Dorsal is up. TH, tyrosine hydroxylase. Scale bars: 10 μm.

2.5. Cultured neurons reveal heterogeneity in their ciliation

Since *in vitro* studies using dissociated neurons and neural explants have been widely used to investigate molecular mechanisms during neurodevelopment, it was important to assess whether primary cilia persisted in these cultures [35].
We first used HH30 DRG primary neurons and cultured them for 1, 2, 5 or 7 days *in vitro* (DIV). We stained them for the neuronal DRG marker Islet-1 and Arl13B to reveal primary cilia (Figure 5A-D). We rarely observed primary cilia in these cultures. In fact, quantifications indicated that the average ciliation rate of DRG neurons was invariably around 20% at all culture times (Figure 5F and Table 1, $p \geq 0.05$). Noteworthy, the large majority of Schwann cells located in DRG, which were co-cultured with DRG neurons and co-stained with 1E8 antibodies, carried a primary cilium already after 1DIV

 doi:10.20944/preprints202102.0031.v1

(white arrowhead, Figure 5E). Quantifications showed that between 80 and 90% of them carried a primary cilium after 1, 2, 5 or 7 DIV without any significant difference between culture times (Figure 5G and Table 1, $p \geq 0.05$). This suggested that the culture conditions were not incompatible with ciliogenesis or cilia maintenance. We then examined the ciliation of HH30 DRG neurons cultured as explants after 1DIV. In contrast to the culture of dissociated cells, we found that the majority of DRG neurons bore a primary cilium (white arrows, Figure 5H). On average 83 ± 2% of Hoechst-positive cells had a primary cilium with 93 ± 1% of these cells being Islet-1-positive DRG neurons (mean ± standard deviation, n = 12 explants, N = 3 replicates).

Preprints (www.preprints.org) | NOT PEER-REVIEWED | Posted: 1 February 2021 doi:10.20944/preprints202102.0031.v1

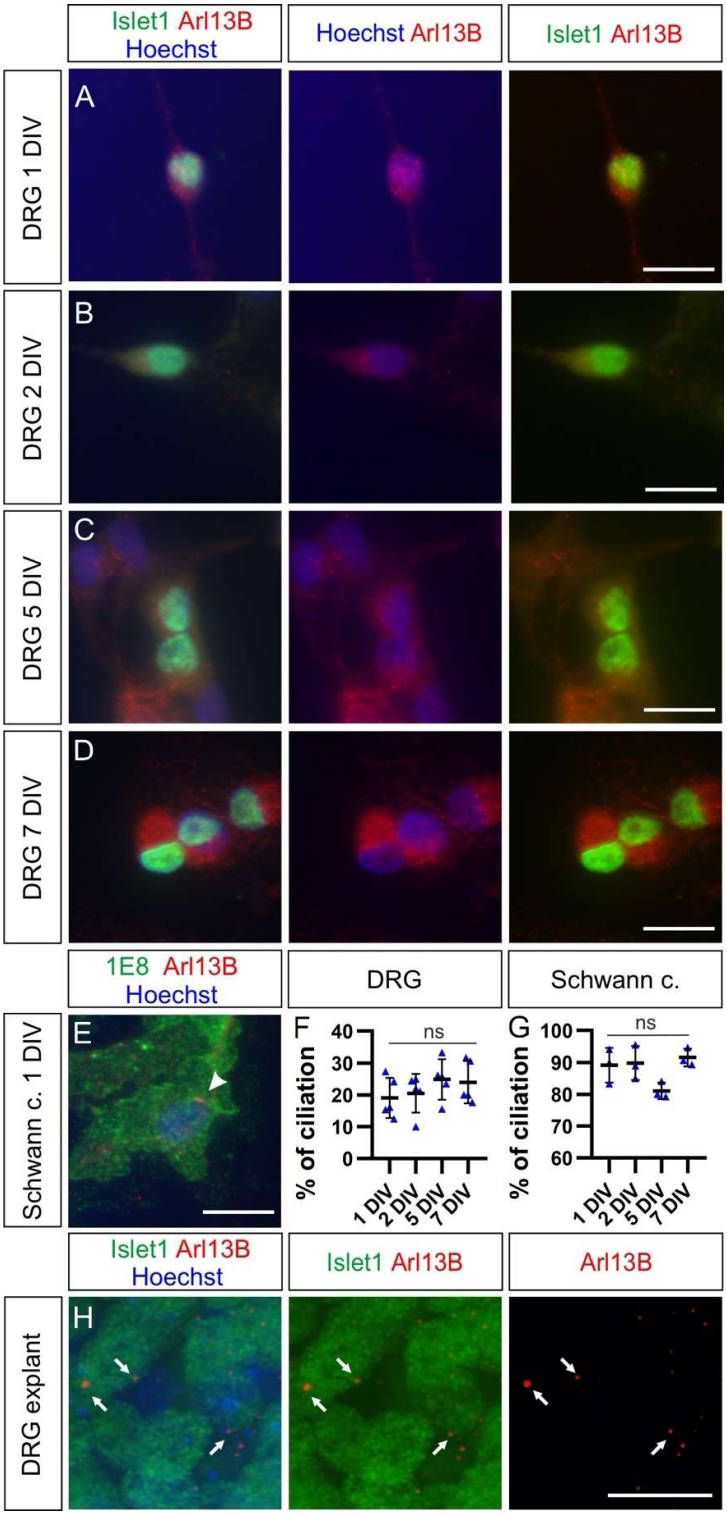

Figure 5. DRG neurons bear a primary cilium in explants, but not in dissociated cultures**. (A-D)** Dissociated DRG neurons cultured for 1, 2, 5, or 7 DIV were stained for Islet1 (green) together with Arl13B (red), revealing primary cilia, and counterstained with Hoechst (blue) to visualization nuclei. No clear ciliary structures could be seen on these cells. **(E)** Most Schwann cells possessed a primary cilium in dissociated cell culture (white arrowhead). **(F,G)** Quantification of the average percentage of ciliation in dissociated cultures of DRG neurons and Schwann cells up to one week of culture. Error bars represent standard deviations. Kruskal–Wallis test with Dunn's multiple-comparisons test (F) and One-way ANOVA with Dunn's multiple-comparisons test (G). $p \geq 0.05$, ns. **(H)**

Preprints (www.preprints.org) | NOT PEER-REVIEWED | Posted: 1 February 2021 doi:10.20944/preprints202102.0031.v1

Islet1-positive DRG neurons in DRG explants possessed a primary cilium (red) after 1DIV (white arrows). Schwann c., Schwann cells. Scale bars: 15 μm .

Table 1. Percentage of ciliation of dissociated neurons. Detailed values for Figure 5 and 6.

	DRG				***Schwann cells***			
	1 DIV	2 DIV	5 DIV	7 DIV	1 DIV	2 DIV	5 DIV	7 DIV
average:	19%	20%	25%	24%	89%	90%	81%	92%
standard deviation:	6%	6%	6%	7%	5%	5%	3%	3%
N(replicates):	5	5	5	5	3	3	3	3
	Commissural neurons				***Motor neurons***			
	1 DIV	2 DIV	5 DIV	7 DIV	1 DIV	2 DIV	5 DIV	7 DIV
average:	66%	68%	66%	76%	48%	47%	80%	85%
standard deviation:	4%	6%	7%	5%	8%	4%	9%	7%
N(replicates):	4	4	4	4	6	6	4	4

As DRG neurons belong to the PNS and could not consistently regain a primary cilium when cultured as dissociated neurons, we assessed and compared the ciliation rate of CNS neurons in culture. As seen for DRG neurons *in vivo*, spinal cord neurons carried a cilium *in vivo* at HH26. We found a primary cilium on most of the dorsally-located Contactin-2/Axonin-1-positive commissural neurons and the ventrally-located Islet-1-positive motoneurons (white arrows, Figure 6A,C). Robust ciliation was still observed in both motoneurons and commissural neurons cultured as explants (white arrows, Figure 6B,D). Interestingly, the ciliation of dissociated motoneurons was around 50% after 1 and 2 DIV, then significantly increased up to around 80% after 5DIV and stayed at a similar level after 7 DIV (Figure 6G and Table 1, $p<0.0001$). In contrast, the majority (~66%) of dissociated commissural neurons carried a primary cilium already after 1 DIV and maintained it at a similar level up to 7 DIV (Figure 6H and Table 1, $p\geq0.05$).

Taken together, our culture experiments showed that DRG neurons are only robustly ciliated when cultured as explants, whereas they did not seem to regain a primary cilium when cultured as dissociated cells. Moreover, the comparison with other neuronal populations from the CNS suggested a better ciliation in dissociated cultures compared to the PNS-located DRG neurons.

Preprints (www.preprints.org) | NOT PEER-REVIEWED | Posted: 1 February 2021 doi:10.20944/preprints202102.0031.v1

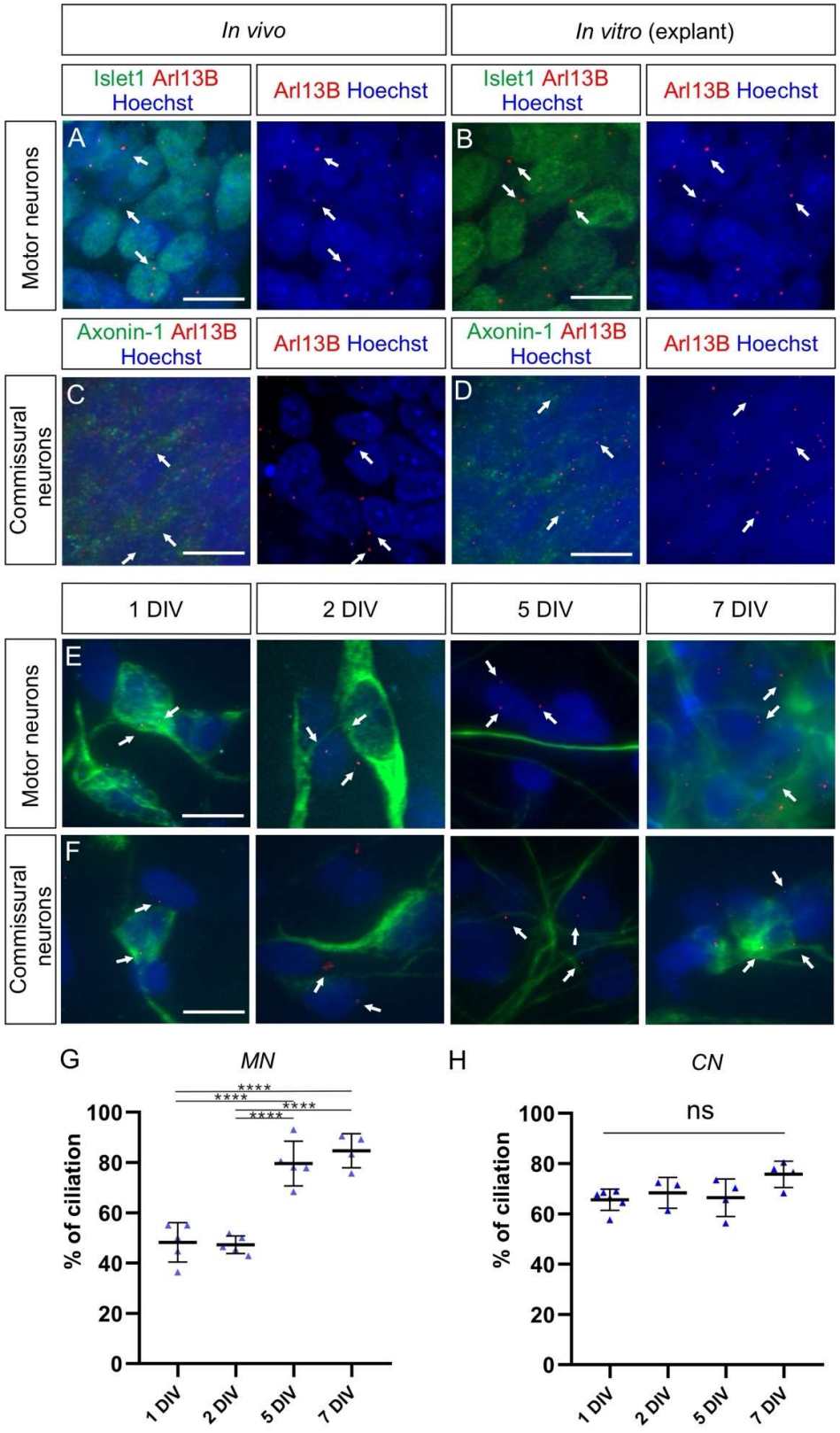

Figure 6. Commissural neurons and motor neurons possessed a primary cilium *in vivo* and in explants cultures, but the ciliation rate was distinct for each population in dissociated cell cultures. **(A)** Islet-1-positive motoneurons located in the ventral horn of the spinal cord bore a primary cilium at HH26 *in vivo* (white arrows). **(B)** Motoneurons also possessed a primary cilium in explants cultured for 1DIV (white arrows). **(C)** Axonin-1-

 doi:10.20944/preprints202102.0031.v1

positive commissural neurons located in the dorsal horn of the spinal cord carried a primary cilium at HH26 *in vivo* (white arrows). **(D)** Commissural neurons also possessed a primary cilium in explants cultured for 1DIV (white arrows). **(E,F)** Cultured dissociated motoneurons (E) and commissural neurons (F) stained for neurofilament (NF-M) carried a primary cilium stained with Arl13B at different levels after 1, 2, 5 and 7 DIV (white arrows). **(G)** About half of the dissociated motoneurons carried a primary cilium after 1 and 2 DIV and the ciliation rate significantly increased up to around 80% after 5 and 7 DIV. One-way ANOVA with Dunn's multiple-comparisons test. **(H)** More than 65% of cultured dissociated commissural neurons carried a primary cilium after 1 DIV and kept it to a similar level up to 7 DIV. Kruskal–Wallis test with Dunn's multiple-comparisons test. Error bars represent standard deviations. $p \geq 0.05$, ns; $p < 0.0001$, ****. MN, motoneurons; CN, commissural neurons. Scale bars: 10 μm.

3. Discussion

In this study, we analyzed the presence of primary cilia in different cell populations of the developing chicken PNS between HH16 and HH30 *in vivo*. Our data showed that NCC and their derivatives carried a primary cilium during early and later stages of the PNS formation (Figure 1-4 and Supplementary Figure 1,2).

We could see that migrating NCC carried a primary cilium while migrating to their final locations where they settle and differentiate (Figure 1). This observation suggests that already at a very early stage of trunk PNS formation, the primary cilium might potentially play a role in the migration and the correct settlement of the NCC. Interestingly, in human ciliopathies, patients have very often an abnormal development of the craniofacial complex which suggests aberrant cranial NCC migration [36]. In line with this, studies using animal models of ciliopathies suggested that cranial NCC migration and development are impaired in a cell-autonomous manner when primary cilia are compromised. A lack of a functional primary cilium led to defects in the development of several organs, such as cranial bone structures, the tongue, and the submandibular gland [37–41]. Interestingly, NCC development at the trunk level involve signaling pathways, such as Wnt, Sonic hedgehog, TGFβ, or chemokine signaling, which are linked to the primary cilium or have components that were shown to localize in it in other cell types [42–46]. Thus, a cell-autonomous role for primary cilia in early NCC development in the trunk is very likely.

Secondly, we described the ciliation of differentiated sensory neurons within the DRG (Figure 2). DRG neurons connect the periphery to the CNS. According to our findings, they were ciliated at all the key stages: when they polarize (HH18), send central afferents into the CNS and peripheral axons toward the periphery (HH26), and when they produce collaterals growing within the deeper layers of the spinal cord (HH30, Figure 2A, B and C, respectively) [47,48]. Interestingly, silencing of the Joubert syndrome protein C5orf42 (also termed CPLANE1 or Jbts17) − a protein required for ciliogenesis − in chicken NCC and neural tube led to obvious defects in the development of DRG central afferents and sciatic nerve development suggesting that a functional primary cilium might play a role in the development of DRG axons both at the periphery and at the central afferent level [21]. Furthermore, the loss of Bardet–Biedl syndrome proteins in the mouse was shown to lead to an alteration in sensory innervation in the skin, suggesting an abnormal development of the peripheral sensory axons in ciliopathies [22]. Therefore, our results will be useful for further investigating the possible roles of a functional primary cilium in sensory neuron axonogenesis, axon guidance, and axon branching *in vivo* given the fact that the DRG system is a very accessible system to study each one of these steps.

Another important population of NCC derivatives that we analyzed were the BCC. BCC bore a primary cilium at both the ventral and dorsal roots as soon as they clustered and maintained their cilium at least until HH30 (Figure 3 and Supplementary Figure 2). Several studies demonstrated a role for these cells as a "gatekeeper" at the CNS-PNS boundary at the ventral root level by maintaining the soma of motoneurons in the ventral spinal cord by Semaphorin 6A-mediated repulsive signals [32,49,50]. In the dorsal roots they might play a role in orchestrating the correct guidance of DRG central afferents into the spinal cord in higher vertebrates [49, 51]. Interestingly, after C5orf42 knock-down in neural crest cells and neural tube, dorsal roots formation and DRG patterning was aberrant [21]. It is possible that such phenotypes result from defects in clustering of

 doi:10.20944/preprints202102.0031.v1

these cells at the dorsal roots. Further experiments will be needed to verify this possibility. BCC also serve as stem cell niche and some of them keep proliferating after clustering [51]. In fact BCC contribute to subtypes of sensory neurons, Schwann cell precursors, and pericytes [33]. Therefore, it will be interesting to study in detail, whether proliferating BCC bear a primary cilium and whether a functional primary cilium would be required for their proliferation as it was shown for granule neuron progenitors of the developing cerebellum [52].

Additionally, to complement these results, we could also detect primary cilia on SG neurons and melanocytes at early stages (Figure 4 and Supplementary Figure 3). As for DRG neurons, the presence of the primary cilium during the development of SG neurons might be of interest, although no hints at a possible role during their development has been reported yet.

Finally, we assessed the ciliation of different populations of neurons *in vitro*. We found that the widely used dissociated embryonic DRG neurons did not consistently recover their primary cilium in culture even after 7 DIV (Figure 5E-G). This was contrasting with previous data showing ciliation of P0 mouse hippocampal neurons after such a time in culture (Figure 5E-G) [53]. However, the majority of DRG neurons cultured as explants for 1 DIV was ciliated (Figure 5H). DRG neurons have been widely used to decipher molecular mechanisms of axonal outgrowth, axon guidance, and branching *in vitro* [54–56]. Interestingly, some of the major guidance receptors, such as Robo1 and Neuropilin-1 have recently been localized to the primary cilium of neurons in the CNS and mouse fibroblasts, respectively [42,57]. Hence, it is possible that some of the signaling pathways involved in axonal development might be transduced at the primary cilium level. Our results stressed the fact that for *in vitro* studies investigating signaling pathways that might involve the primary cilium, the proper culture system should be carefully chosen. In the case of embryonic DRG neurons, DRG explant rather than dissociated cultures should be preferentially used.

Furthermore, we could also detect heterogeneity in the ciliation of CNS neurons compared to DRG neurons. The majority of commissural neurons and motoneurons carried a primary cilium when cultured as explants, as it was the case for DRG neurons (Figure 6A-D). Dissociated commissural neurons were robustly ciliated already after 1 DIV but motoneurons only after 5 DIV (Figure 6E-H). This suggested differences in the capacity for ciliogenesis *in vitro* among these neuronal cell types once they are dissociated: from being fast (commissural neurons), to slow (motoneurons), to inefficient (DRG neurons) in rebuilding a primary cilium. These differences might be due to changes in the expression of genes involved in ciliogenesis in specific population of neurons compared to others [58,59].

Overall, the presence of primary cilia in NCC and all their derivatives studied above in the chicken embryo *in vivo* prompts further research to explore the role that the primary cilium might play during PNS formation. In particular, *in ovo* RNAi-based knockdown or CRISPR/Cas9-based knockout of specific genes will help to address these questions in more details in the chicken [60–63]. Our results pave the way for further studies utilizing the chicken embryo as a model for deciphering the potential role for the primary cilium in neural circuit formation in the PNS.

4. Materials and Methods

4.1. Embryo dissection and fixation

The developmental stages of the chicken embryos were determined according to Hamburger and Hamilton [64]. The bodies were pinned down with insect pins (stainless steel pins) in a silicon layered dish filled with cold PBS. The internal organs were removed until the vertebrae and the ribs were visible. For fixation, the extremities of older embryos (HH30) were shortened. Embryos were transferred to a new dish and fixed in 4% paraformaldehyde in PBS at room temperature for 1 hour (HH18-HH26) or 2 hours (HH30). Then, they were washed 3 times for 10 minutes with PBS at RT. For cryoprotection of the tissue, embryos were transferred to 25% sucrose in PBS and incubated for at least 24 hours at 4°C. For cryosectioning, the tissue was embedded in O.C.T. compound (Tissue-Tek), frozen and cut with a thickness of 25 µm with a cryostat (Leica CM1850).

 doi:10.20944/preprints202102.0031.v1

4.2. In ovo electroporation

In ovo electroporation was used to target neural crest cells in HH12-14 embryos as described previously [65,66]. A DNA mix containing 25 ng/µl β-actin::hrGFPII and 25 ng/µl β-actin::Arl13B-RFP plasmids [67] diluted in in PBS and 0.1% Fast Green was injected into the central canal of the neural tube and unilaterally electroporated using a BTX ECM830 square-wave electroporator (five pulses at 18 V with 50 ms duration each and 1 sec interpulse interval), as previously described [66]. Eggs were then incubated for 3 more days at 39°C until embryos reached stage HH26.

4.3. Immunohistochemistry

To prevent unspecific antibody binding, transverse spinal cord sections were incubated in blocking buffer (5% FCS in PBS) containing 0.25% Triton X-100 for one hour in a humid chamber. They were then washed 3x for 10 min each with PBS containing 0.25% Triton X-100 at room temperature. Primary antibody mixtures were prepared in blocking buffer and added to the slides (Table 2). Slides were incubated overnight at 4°C in a humid chamber.

Table 2. List of primary antibodies used for immunohistochemistry and immunocytochemistry.

Antigen	Species	Source	Cat#	Dilution
Arl13B	Rabbit (polyclonal)	Proteintech Group	13967-1-AP, RRID:AB_2121979	1:1000
Ift88	Rabbit (polyclonal)	Proteintech Group	17711-1-AP, RRID:AB_2060867	1:1000
Islet1 (clone 40.2D6)	Mouse (monoclonal)	DSHB	40.2D6, RRID:AB_528315	1:30 (supernatant)
MelEM	Mouse (monoclonal)	DSHB	MelEM RRID:AB_531849	1:2 (supernatant)
P0 (clone 1E8)	Mouse (monoclonal)	DSHB	1E8 RRID:AB_2078498	1:2 (supernatant)
HNK1 (clone 1C10)	Mouse (monoclonal)	DSHB	1C10 RRID:AB_10570406	1:2 (supernatant)
Axonin-1/Contactin-2	Goat (polyclonal)	Sonderegger Lab	NA	1:1000
Tyrosine Hydroxylase	Mouse (monoclonal)	DSHB	aTH RRID:AB_528490	1:5 (supernatant)
Neurofilament-M (clone RMO270)	Mouse (monoclonal)	Invitrogen (Zymed)	RMO270 RRID:AB_2315286	1:250

The next day, the spinal cord sections were washed 3x for 10 min each at room temperature with PBS/0.25% Triton X-100. Afterwards, secondary antibodies diluted in blocking buffer were added to each slide (Table 3). The slides were then incubated for 2 h in a humid chamber at room temperature protected from light. Before mounting, sections were counterstained with Hoechst (Invitrogen, Catalog number H3570, 2.5 µg/ml in PBS) for 10 min at room temperature followed by 3x 10 min each washing with PBS/0.25% Triton X- 100 and 2x for 5 min each with PBS at room temperature. Afterwards, slides were either mounted with Mowiol/DABCO, or further stained for primary cilia with the protocol outlined below.

 doi:10.20944/preprints202102.0031.v1

4.4. Immunohistochemistry for primary cilia

Importantly, to stain primary cilia in the PNS, no detergent was used and primary cilia were stained with rabbit anti-Arl13B antibody (Proteintech) diluted at 1:1000 in 5% FCS in PBS for 2 h at room temperature (Table 3). This brief incubation time resulted in an increased ratio of ciliary versus extra-ciliary staining of Arl13B. Following this incubation, slides were washed 3 times with PBS for 10 min each and a secondary antibody (donkey-anti-rabbit-Cy3) diluted at 1:1000 in blocking buffer was given to slides for 2 h at room temperature (Table 3). Finally, sections were washed 3x 10 min each with PBS and mounted as described above.

Table 3. List of secondary antibodies used for immunostaining.

Secondary antibodies	Source	Cat#	Dilution
Donkey-anti-mouse IgG-Alexa-488	Invitrogen (Molecular Probes)	A21202 RRID:AB_141607	1:1000
Donkey-anti-rabbit-Cy3	Jackson ImmunoResearch	715-165-152 RRID: AB_2307443	1:1000
Donkey-anti-goat-Cy5	Jackson ImmunoResearch	705-175-147 RRID: AB_2340415	1:1000
Donkey-anti-Goat IgG-Alexa-488	Invitrogen (Molecular Probes)	A11055 RRID:AB_2534102	1:1000

4.5. Cultures of dissociated neurons

For accessing the DRG, HH30 embryos were pined down as described for immunohistochemistry and the ventral vertebrae and the spinal cord were removed to access DRG. For motoneurons and commissural neurons, open-book preparations of spinal cords dissected from HH26 embryos were used and stripes of tissue were cut at the ventral region (motor column) or the most dorsal region (commissural neurons) of the spinal cord with small spring scissors [66]. Each population was dissociated using a 20 min incubation at 37°C in 0.25% Trypsin in PBS (Invitrogen, cat# 15090-046) containing DNase (Roche, cat# 101 041 590 01; final concentration: 0.2%) followed by pelleting by centrifugation (5 min, 1000 rpm, room temperature) and trituration with a fire-polished Pasteur pipette in culture media. Finally, cells were resuspended in the respective culture medium (Table 4). N3 supplement was added to a final concentration of 100 µg/ml transferrin, 10 µg/ml insulin, 20 ng/ml triiodothyronine, 40 nM progesterone, 200 ng/ml corticosterone, 200 µM putrescine, 60 nM sodium selenite (all from Sigma). Penicillin and Streptomycin (Invitrogen, cat# 15140-122) were added to the media for a final concentration of 100 Units/ml and 100 µg/ml, respectively. Cells were plated in 8-well Lab-Tek plates (20'000 cells per well; Nunc, cat# 177445) and cultured for the desired time at 37°C with 5% CO_2. Lab-Tek plates were pre-coated with poly-L-Lysine (20 µg/ml, Sigma cat# P-12374) and coated with 10 µg/ml Laminin (Invitrogen, cat# 23017-015). When neurons were cultured for more than 2 days, fresh medium was added every two days (half of the volume of old medium in the well was exchanged with the fresh one).

Preprints (www.preprints.org) | NOT PEER-REVIEWED | Posted: 1 February 2021 doi:10.20944/preprints202102.0031.v1

Table 4. Media contents for different cell populations in dissociated cell cultures and explants.

Cell Populations				
DRG	MEM with Glutamax (Invitrogen, cat# 41090-028)	Albumax (4 mg/ml, Invitrogen; cat# 11020-021)	N3	NGF (20 ng/ml; Invitrogen; cat# 13290-010)
Commissural neurons/motor neurons	MEM with Glutamax (Invitrogen, cat# 41090-028)	Albumax (4 mg/ml, Invitrogen; cat# 11020-021)	N3	Pyruvate (1 mM; Sigma; cat# P5280)

Cells were fixed after 1, 2, 5, or 7 DIV by adding one volume of pre-warmed 4% PFA in PBS to each well and incubation for 5 min at 37° C with 5% CO_2. Then, the medium-PFA mix was exchanged for pre-warmed 4% PFA in PBS and cells were incubated for another 15 min with the same conditions, before being washed with PBS at room temperature.

4.6. Explants cultures

For explant cultures, LabTek wells were pre-coated with poly-L-Lysine and Laminin as described above. Explants of DRG, motoneurons or commissural neurons were transferred directly into LabTek wells containing a total of 400 µl medium (Table 4). After 1DIV, 400 µl of pre-warmed 2% PFA with 15% sucrose in PBS (fixation buffer) were added to gently fix the explants, as described previously [68]. Following 40 min of incubation at room temperature, the upper phase of the solution (200 µl) was discarded and 200 µl of fresh fixation buffer was given. After incubation for another hour, the explants were washed 3x 10 min each with PBS at room temperature.

4.7. Immunocytochemistry

Cells were permeabilized with 0.1% Triton-X 100 in PBS (for dissociated neurons) or 0.25% Triton-X 100 in PBS (for explants) for 4 min at room temperature. They were rinsed 3x for 5 min each with PBS and blocked 15 min with 5% FCS in PBS (blocking buffer) at room temperature. Primary antibodies were diluted in blocking buffer and added to the cells for 1 h at room temperature (Table 2). Cells were washed again with PBS and incubated in secondary antibodies diluted in blocking buffer for 1 h at room temperature (Table 3). Cells were counterstained with Hoechst (2.5 µg/ml in PBS, Cat#H3570 Invitrogen) for 4 min at RT and rinsed 3x 5 min each with PBS before mounting as described above.

4.8. Microscopy

Images were taken with an Olympus BX61 upright microscope equipped with a spinning disk unit (BX-DSU, Olympus) and a 10x air objective (UPLFL PH 10x/0.30, Olympus), 40x water objective (UAPO W/340 40x/1.15, Olympus) or a 60x oil objective (PLAPON O 60x/1.42, Olympus) and an Orca-R^2 camera (Hamamatsu) with the Olympus CellSens Dimension 2.2 software. Cilia were visualized with 60x or 40x objective and images were acquired with 20 planes for 40x images with 0.32 µm distance between planes. For 10x and 60x images 3.54 µm and 0.24 µm distance were applied, respectively. The number of planes was variable. High magnification images were 2D deconvolved (nearest neighbor) using the Olympus CellSens Dimension 2.2 software. Maximum intensity z-projection were created with the same software and all images were analyzed and equally modified in Fiji/ImageJ [69].

 doi:10.20944/preprints202102.0031.v1

4.9. Quantification of ciliation

To quantify the number of primary cilia in HH26 DRG *in vivo* and HH30 explants in vitro, Fiji/ImageJ was used with images acquired with the 40x objective. First, a 2-channel picture with Islet1 (green) and Arl13B (red) was split into separate channels (Figure 7A). On the picture displaying the primary cilia (Arl13B, red), "Triangle" threshold was applied (Figure 7B). The picture showing the Islet1-positive DRG neurons was used to select the region of interest of the DRG with the freehand selections tool (Figure 7C). This selection was transferred to the thresholded primary cilia picture (Figure 7D). Finally, cilia were automatically counted within the region of interest using the 'count particles' options (0-1 circularity, 0.2 μm^2 minimum size, Figure 7E).The number of Hoechst-positive and Islet-1-positive cells in the region of interest was counted manually to calculate the percentage of ciliation within each DRG. To quantify the percentage of ciliation in dissociated cultures, the numbers of total and ciliated neurons/cells per picture were manually counted by an experimenter blind to the experimental conditions using Fiji/ImageJ. The percentage of ciliation per replicate was calculated as the average from 4 adjacent pictures taken in the center of the well.

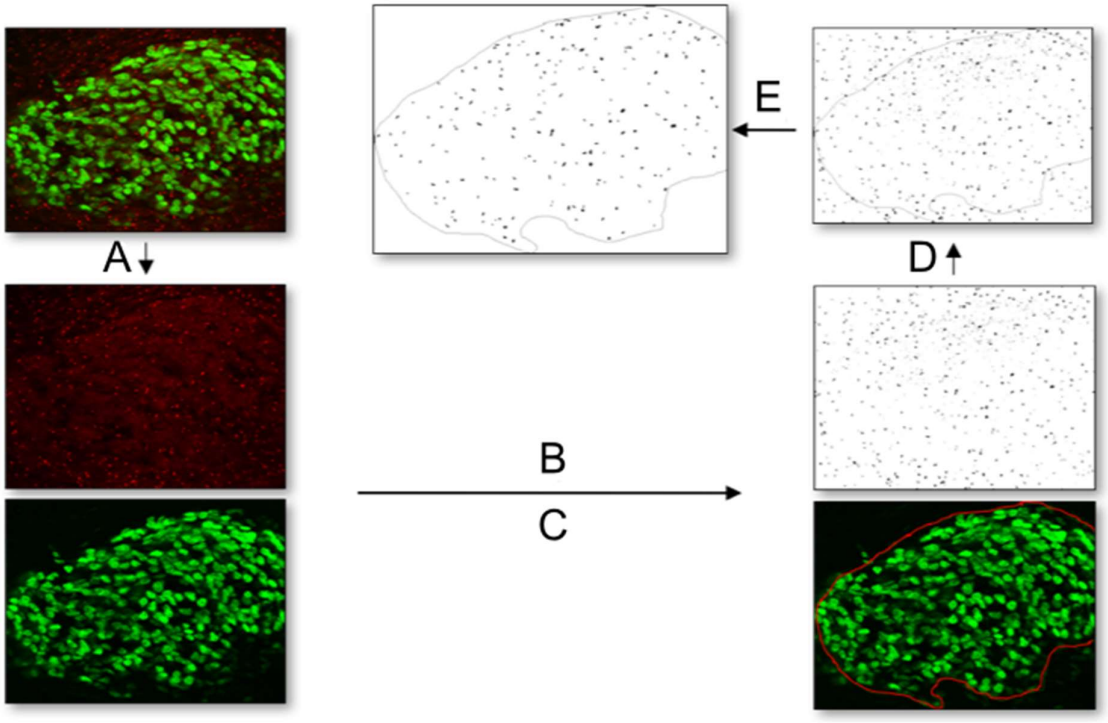

Figure 7. Workflow for quantification of primary cilia with the image analysis program Fiji. **(A)** First, a 2-channel picture with Islet1 (green) and Arl13B (red) was split into separate channels. **(B)** On the picture displaying the primary cilia (Arl13B, red), "Triangle" threshold was applied. **(C)** The picture showing the Islet1-positive DRG neurons was used to select the region of interest of the DRG with the freehand selection tool. **(D)** This selection was transferred to the thresholded primary cilia picture. **(E)** Finally, cilia were automatically counted within the region of interest using the 'count particles' options.

4.10. Statistical analysis

Statistical analyses were carried out using GraphPad Prism 8 software. All data were assessed for normality (normal distribution) using the D'Agostino and Pearson omnibus K2 normality test and visual assessment of the normal quantile–quantile plot before choosing an appropriate (parametric or nonparametric) statistical test. All tests used in this study are mentioned either in the text or in the legend of figures.

Author Contributions: Conceptualization, A.D. and E.T.S.; methodology, E.Y. and A.D; formal analysis, E.Y. and A.D.; investigation, E.Y. and A.D.; writing—original draft preparation, E.Y. and A.D.; writing—review and editing, E.Y., A.D. and E.T.S.; supervision, E.T.S..; project administration, E.T.S.; funding acquisition, E.T.S..

Funding: Swiss National Science Foundation.

Acknowledgments: We thank Dr. Raman Das (University of Manchester) for the Arl13B-RFP construct. We thank Alexander Hess for helping collect preliminary data *in vivo*.

Conflicts of Interest: The authors declare no conflict of interest. The funders had no role in the design of the study; in the collection, analyses, or interpretation of data; in the writing of the manuscript, or in the decision to publish the results.

Abbreviations

CNS	central nervous system
PNS	peripheral nervous system
DRG	dorsal root ganglia
BCC	boundary cap cells
NCC	neural crest cells
SG	sympathetic ganglia
HH	Hamburger and Hamilton stage
DIV	day in vitro

Appendix A

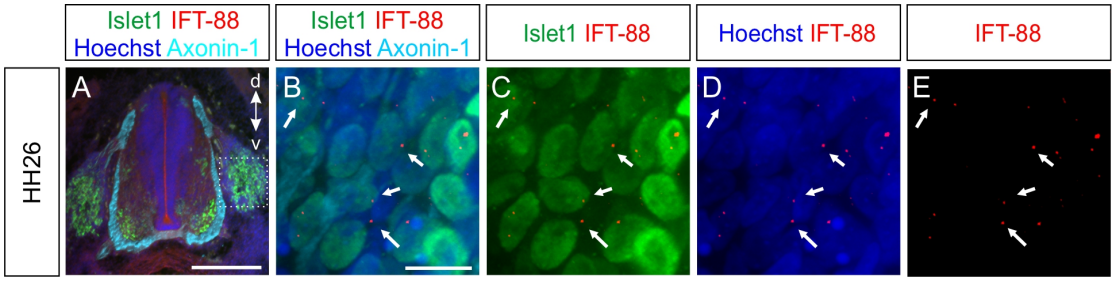

Supplementary Figure 1. Confirmation of the presence of a primary cilium on DRG neurons with IFT88 staining. IFT88 is a component of the intraflagellar transport complex **(A)** Overview and **(B-E)** high-magnification images of DRG neurons from transverse sections of HH26 embryos stained for Islet-1 (green), IFT88 (red), Contactin-2/Axonin-1 (cyan) and counterstained with Hoechst (blue). **(B-E)** IFT88 staining confirmed that Islet-1-positive DRG neurons bore a primary cilium (white arrows). d, dorsal; v, ventral. Scale bars: 250 μm (A) and 10 μm (B-E).

Preprints (www.preprints.org) | NOT PEER-REVIEWED | Posted: 1 February 2021 doi:10.20944/preprints202102.0031.v1

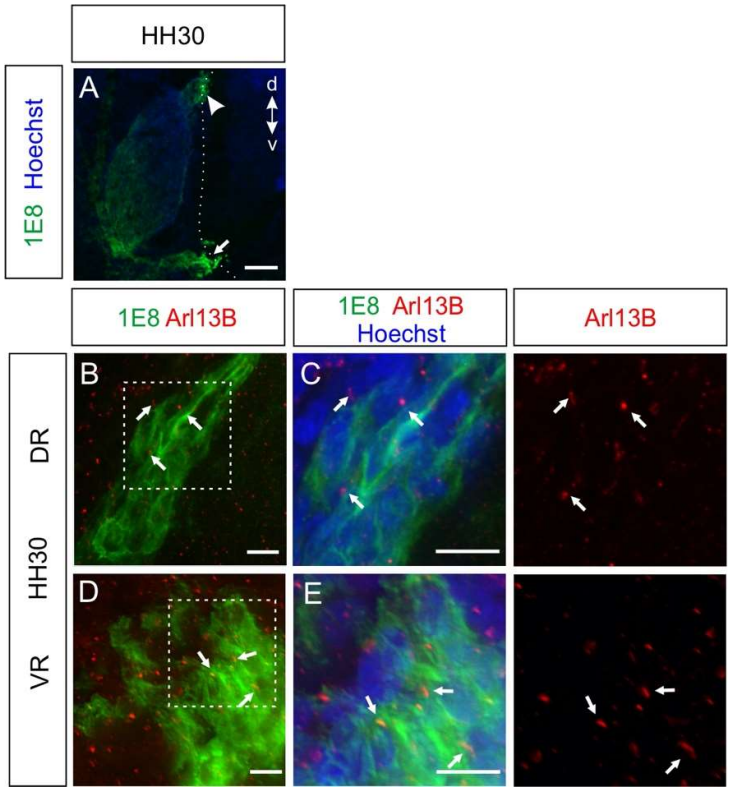

Supplementary Figure 2. Boundary Cap Cells (BCC) carried a primary cilium at HH30, both in dorsal and ventral roots. **(A)** 1E8-positive BCC cluster (green) localized at the dorsal root (DR, arrowhead) and the ventral root (VR, arrow). High-magnification micrographs of BCC at DR **(B-C)** and VR **(D-E)** co-labeled with Arl13B (red) revealed that these cells carried a primary cilium at HH30 (white arrows). Dashed line in A represents the boundary of the spinal cord. Squares with dashed lines represent the region of interest in the right panels. d, dorsal; v, ventral; VR, central roots; DR, dorsal roots. Scale bars: 100 μm (A) and 10 μm (B-E).

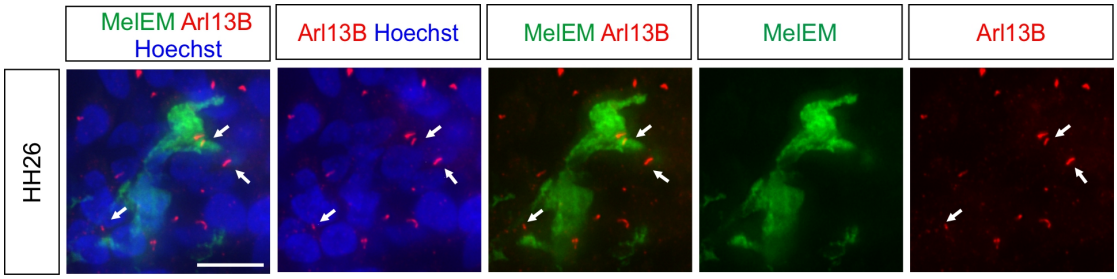

Supplementary Figure 3. Other NCC derivatives such as melanocytes possessed a primary cilium *in vivo*. MelEM stained melanocytes (green) and Arl13B (red) visualized primary cilia (arrows). Hoechst stained nuclei (blue). Stage: HH26. Scale bar: 10 μm.

References

1. Broekhuis, J.R.; Leong, W.Y.; Jansen, G. Regulation of Cilium Length and Intraflagellar Transport. In *International Review of Cell and Molecular Biology*; Elsevier, 2013; Vol. 303, pp. 101–138 ISBN 978-0-12-407697-6.
2. Gerdes, J.M.; Davis, E.E.; Katsanis, N. The Vertebrate Primary Cilium in Development, Homeostasis, and Disease. *Cell* **2009**, *137*, 32–45, doi:10.1016/j.cell.2009.03.023.
3. Oh, E.C.; Katsanis, N. Cilia in Vertebrate Development and Disease. *Development* **2012**, *139*, 443–448, doi:10.1242/dev.050054.

4. Zimmermann, K.W. Beiträge zur Kenntniss einiger Drüsen und Epithelien: Hierzu Tafel XXVII, XXVIII u. XXIX. *Archiv f. mikrosk. Anat.* **1898**, *52*, 552–706, doi:10.1007/BF02975837.
5. Wong, S.Y.; Reiter, J.F. The Primary Cilium at the Crossroads of Mammalian Hedgehog Signaling. *Curr Top Dev Biol* **2008**, *85*, 225–260, doi:10.1016/S0070-2153(08)00809-0.
6. Huangfu, D.; Anderson, K.V. Cilia and Hedgehog Responsiveness in the Mouse. *Proc Natl Acad Sci U S A* **2005**, *102*, 11325–11330, doi:10.1073/pnas.0505328102.
7. Otto, E.A.; Schermer, B.; Obara, T.; O'Toole, J.F.; Hiller, K.S.; Mueller, A.M.; Ruf, R.G.; Hoefele, J.; Beekmann, F.; Landau, D.; et al. Mutations in INVS Encoding Inversin Cause Nephronophthisis Type 2, Linking Renal Cystic Disease to the Function of Primary Cilia and Left-Right Axis Determination. *Nat Genet* **2003**, *34*, 413–420, doi:10.1038/ng1217.
8. Simons, M.; Gloy, J.; Ganner, A.; Bullerkotte, A.; Bashkurov, M.; Krönig, C.; Schermer, B.; Benzing, T.; Cabello, O.A.; Jenny, A.; et al. Inversin, the Gene Product Mutated in Nephronophthisis Type II, Functions as a Molecular Switch between Wnt Signaling Pathways. *Nat Genet* **2005**, *37*, 537–543, doi:10.1038/ng1552.
9. Schneider, L.; Clement, C.A.; Teilmann, S.C.; Pazour, G.J.; Hoffmann, E.K.; Satir, P.; Christensen, S.T. PDGFRalphaalpha Signaling Is Regulated through the Primary Cilium in Fibroblasts. *Curr Biol* **2005**, *15*, 1861–1866, doi:10.1016/j.cub.2005.09.012.
10. Schmid, F.M.; Schou, K.B.; Vilhelm, M.J.; Holm, M.S.; Breslin, L.; Farinelli, P.; Larsen, L.A.; Andersen, J.S.; Pedersen, L.B.; Christensen, S.T. IFT20 Modulates Ciliary PDGFRα Signaling by Regulating the Stability of Cbl E3 Ubiquitin Ligases. *Journal of Cell Biology* **2018**, *217*, 151–161, doi:10.1083/jcb.201611050.
11. Boehlke, C.; Kotsis, F.; Patel, V.; Braeg, S.; Voelker, H.; Bredt, S.; Beyer, T.; Janusch, H.; Hamann, C.; Gödel, M.; et al. Primary Cilia Regulate MTORC1 Activity and Cell Size through Lkb1. *Nat Cell Biol* **2010**, *12*, 1115–1122, doi:10.1038/ncb2117.
12. Satir, P.; Pedersen, L.B.; Christensen, S.T. The Primary Cilium at a Glance. *J Cell Sci* **2010**, *123*, 499–503, doi:10.1242/jcs.050377.
13. Mitchison, H.M.; Valente, E.M. Motile and Non-Motile Cilia in Human Pathology: From Function to Phenotypes: Motile and Non-Motile Ciliopathies. *J. Pathol.* **2017**, *241*, 294–309, doi:10.1002/path.4843.
14. Lee, J.E.; Gleeson, J.G. A Systems-Biology Approach to Understanding the Ciliopathy Disorders. *Genome Med* **2011**, *3*, 59, doi:10.1186/gm275.
15. Ware, S.M.; Aygun, M.G.-; Hildebrandt, F. Spectrum of Clinical Diseases Caused By Disorders of Primary Cilia. *Proceedings of the American Thoracic Society* **2011**, *8*, 444–450, doi:10.1513/pats.201103-025SD.
16. Hildebrandt, F.; Benzing, T.; Katsanis, N. Ciliopathies. *N Engl J Med* **2011**, *364*, 1533–1543, doi:10.1056/NEJMra1010172.
17. Grochowsky, A.; Gunay-Aygun, M. Clinical Characteristics of Individual Organ System Disease in Non-Motile Ciliopathies. *TRD* **2019**, *4*, 1–23, doi:10.3233/TRD-190033.
18. Guemez-Gamboa, A.; Coufal, N.G.; Gleeson, J.G. Primary Cilia in the Developing and Mature Brain. *Neuron* **2014**, *82*, 511–521, doi:10.1016/j.neuron.2014.04.024.
19. Suciu, S.K.; Caspary, T. Cilia, Neural Development and Disease. *Seminars in Cell & Developmental Biology* **2020**, S1084952119301727, doi:10.1016/j.semcdb.2020.07.014.
20. Métin, C.; Pedraza, M. Cilia: Traffic Directors along the Road of Cortical Development. *Neuroscientist* **2014**, *20*, 468–482, doi:10.1177/1073858414543151.
21. Asadollahi, R.; Strauss, J.E.; Zenker, M.; Beuing, O.; Edvardson, S.; Elpeleg, O.; Strom, T.M.; Joset, P.; Niedrist, D.; Otte, C.; et al. Clinical and Experimental Evidence Suggest

a Link between KIF7 and C5orf42-Related Ciliopathies through Sonic Hedgehog Signaling. *Eur J Hum Genet* **2018**, *26*, 197–209, doi:10.1038/s41431-017-0019-9.

22. Tan, P.L.; Barr, T.; Inglis, P.N.; Mitsuma, N.; Huang, S.M.; Garcia-Gonzalez, M.A.; Bradley, B.A.; Coforio, S.; Albrecht, P.J.; Watnick, T.; et al. Loss of Bardet Biedl Syndrome Proteins Causes Defects in Peripheral Sensory Innervation and Function. *Proceedings of the National Academy of Sciences* **2007**, *104*, 17524–17529, doi:10.1073/pnas.0706618104.
23. Etchevers, H.C.; Dupin, E.; Le Douarin, N.M. The Diverse Neural Crest: From Embryology to Human Pathology. *Development* **2019**, *146*, dev169821, doi:10.1242/dev.169821.
24. Theveneau, E.; Mayor, R. Neural Crest Delamination and Migration: From Epithelium-to-Mesenchyme Transition to Collective Cell Migration. *Developmental Biology* **2012**, *366*, 34–54, doi:10.1016/j.ydbio.2011.12.041.
25. Theveneau, E.; Mayor, R. Neural Crest Delamination and Migration: From Epithelium-to-Mesenchyme Transition to Collective Cell Migration. *Developmental Biology* **2012**, *366*, 34–54, doi:10.1016/j.ydbio.2011.12.041.
26. Marmigère, F.; Ernfors, P. Specification and Connectivity of Neuronal Subtypes in the Sensory Lineage. *Nat Rev Neurosci* **2007**, *8*, 114–127, doi:10.1038/nrn2057.
27. Giovannone, D.; Ortega, B.; Reyes, M.; El-Ghali, N.; Rabadi, M.; Sao, S.; de Bellard, M.E. Chicken Trunk Neural Crest Migration Visualized with HNK1. *Acta Histochemica* **2015**, *117*, 255–266, doi:10.1016/j.acthis.2015.03.002.
28. Caspary, T.; Larkins, C.E.; Anderson, K.V. The Graded Response to Sonic Hedgehog Depends on Cilia Architecture. *Developmental Cell* **2007**, *12*, 767–778, doi:10.1016/j.devcel.2007.03.004.
29. Dumoulin, A.; Schmidt, H.; Rathjen, F.G. Sensory Neurons: The Formation of T-Shaped Branches Is Dependent on a CGMP-Dependent Signaling Cascade. *Neuroscientist* **2021**, *27*, 47–57, doi:10.1177/1073858420913844.
30. Cole, D.G.; Diener, D.R.; Himelblau, A.L.; Beech, P.L.; Fuster, J.C.; Rosenbaum, J.L. Chlamydomonas Kinesin-II–Dependent Intraflagellar Transport (IFT): IFT Particles Contain Proteins Required for Ciliary Assembly in Caenorhabditis Elegans Sensory Neurons. *Journal of Cell Biology* **1998**, *141*, 993–1008, doi:10.1083/jcb.141.4.993.
31. Perrin, F.E.; Rathjen, F.G.; Stoeckli, E.T. Distinct Subpopulations of Sensory Afferents Require F11 or Axonin-1 for Growth to Their Target Layers within the Spinal Cord of the Chick. *Neuron* **2001**, *30*, 707–723, doi:10.1016/S0896-6273(01)00315-4.
32. Fontenas, L.; Kucenas, S. Livin' On The Edge: Glia Shape Nervous System Transition Zones. *Current Opinion in Neurobiology* **2017**, *47*, 44–51, doi:10.1016/j.conb.2017.09.008.
33. Radomska, K.J.; Topilko, P. Boundary Cap Cells in Development and Disease. *Current Opinion in Neurobiology* **2017**, *47*, 209–215, doi:10.1016/j.conb.2017.11.003.
34. Ernsberger, U.; Rohrer, H. Sympathetic Tales: Subdivisons of the Autonomic Nervous System and the Impact of Developmental Studies. *Neural Dev* **2018**, *13*, 20, doi:10.1186/s13064-018-0117-6.
35. Tojima, T.; Hines, J.H.; Henley, J.R.; Kamiguchi, H. Second Messengers and Membrane Trafficking Direct and Organize Growth Cone Steering. *Nat Rev Neurosci* **2011**, *12*, 191–203, doi:10.1038/nrn2996.
36. Schock, E.N.; Brugmann, S.A. Discovery, Diagnosis, and Etiology of Craniofacial Ciliopathies. *Cold Spring Harb Perspect Biol* **2017**, *9*, a028258, doi:10.1101/cshperspect.a028258.
37. Elliott, K.H.; Millington, G.; Brugmann, S.A. A Novel Role for Cilia-Dependent Sonic Hedgehog Signaling during Submandibular Gland Development: Novel Role for Cilia-

Dependent Shh Signaling During SMG Development. *Dev. Dyn.* **2018**, *247*, 818–831, doi:10.1002/dvdy.24627.

38. Schock, E.N.; Struve, J.N.; Chang, C.-F.; Williams, T.J.; Snedeker, J.; Attia, A.C.; Stottmann, R.W.; Brugmann, S.A. A Tissue-Specific Role for Intraflagellar Transport Genes during Craniofacial Development. *PLoS ONE* **2017**, *12*, e0174206, doi:10.1371/journal.pone.0174206.
39. Tian, H.; Feng, J.; Li, J.; Ho, T.-V.; Yuan, Y.; Liu, Y.; Brindopke, F.; Figueiredo, J.C.; Magee, W.; Sanchez-Lara, P.A.; et al. Intraflagellar Transport 88 (IFT88) Is Crucial for Craniofacial Development in Mice and Is a Candidate Gene for Human Cleft Lip and Palate. *Hum. Mol. Genet.* **2017**, ddx002, doi:10.1093/hmg/ddx002.
40. Millington, G.; Elliott, K.H.; Chang, Y.-T.; Chang, C.-F.; Dlugosz, A.; Brugmann, S.A. Cilia-Dependent GLI Processing in Neural Crest Cells Is Required for Tongue Development. *Developmental Biology* **2017**, *424*, 124–137, doi:10.1016/j.ydbio.2017.02.021.
41. Portal, C.; Rompolas, P.; Lwigale, P.; Iomini, C. Primary Cilia Deficiency in Neural Crest Cells Models Anterior Segment Dysgenesis in Mouse. *eLife* **2019**, *8*, e52423, doi:10.7554/eLife.52423.
42. Higginbotham, H.; Eom, T.-Y.; Mariani, L.E.; Bachleda, A.; Hirt, J.; Gukassyan, V.; Cusack, C.L.; Lai, C.; Caspary, T.; Anton, E.S. Arl13b in Primary Cilia Regulates the Migration and Placement of Interneurons in the Developing Cerebral Cortex. *Developmental Cell* **2012**, *23*, 925–938, doi:10.1016/j.devcel.2012.09.019.
43. Monaco, S.; Baur, K.; Hellwig, A.; Hölzl-Wenig, G.; Mandl, C.; Ciccolini, F. A Flow Cytometry-Based Approach for the Isolation and Characterization of Neural Stem Cell Primary Cilia. *Front. Cell. Neurosci.* **2019**, *12*, 519, doi:10.3389/fncel.2018.00519.
44. Maj, E.; Künneke, L.; Loresch, E.; Grund, A.; Melchert, J.; Pieler, T.; Aspelmeier, T.; Borchers, A. Controlled Levels of Canonical Wnt Signaling Are Required for Neural Crest Migration. *Developmental Biology* **2016**, *417*, 77–90, doi:10.1016/j.ydbio.2016.06.022.
45. Bhatt, S.; Diaz, R.; Trainor, P.A. Signals and Switches in Mammalian Neural Crest Cell Differentiation. *Cold Spring Harb Perspect Biol* **2013**, *5*, doi:10.1101/cshperspect.a008326.
46. Clement, C.A.; Ajbro, K.D.; Koefoed, K.; Vestergaard, M.L.; Veland, I.R.; Henriques de Jesus, M.P.R.; Pedersen, L.B.; Benmerah, A.; Andersen, C.Y.; Larsen, L.A.; et al. TGF-β Signaling Is Associated with Endocytosis at the Pocket Region of the Primary Cilium. *Cell Reports* **2013**, *3*, 1806–1814, doi:10.1016/j.celrep.2013.05.020.
47. Dumoulin, A.; Ter-Avetisyan, G.; Schmidt, H.; Rathjen, F. Molecular Analysis of Sensory Axon Branching Unraveled a CGMP-Dependent Signaling Cascade. *IJMS* **2018**, *19*, 1266, doi:10.3390/ijms19051266.
48. Davis, B.M.; Frank, E.; Johnson, F.A.; Scott, S.A. Development of Central Projections of Lumbosacral Sensory Neurons in the Chick. *J. Comp. Neurol.* **1989**, *279*, 556–566, doi:10.1002/cne.902790405.
49. Mauti, O.; Domanitskaya, E.; Andermatt, I.; Sadhu, R.; Stoeckli, E.T. Semaphorin6A Acts as a Gate Keeper between the Central and the Peripheral Nervous System. *Neural Dev* **2007**, *2*, 28, doi:10.1186/1749-8104-2-28.
50. Bron, R.; Vermeren, M.; Kokot, N.; Andrews, W.; Little, G.E.; Mitchell, K.J.; Cohen, J. Boundary Cap Cells Constrain Spinal Motor Neuron Somal Migration at Motor Exit Points by a Semaphorin-Plexin Mechanism. *Neural Dev* **2007**, *2*, 21, doi:10.1186/1749-8104-2-21.
51. Golding, J.P.; Cohen, J. Border Controls at the Mammalian Spinal Cord: Late-Surviving Neural Crest Boundary Cap Cells at Dorsal Root Entry Sites May Regulate Sensory

Afferent Ingrowth and Entry Zone Morphogenesis. *Molecular and Cellular Neuroscience* **1997**, *9*, 381–396, doi:10.1006/mcne.1997.0647.

52. Chang, C.-H.; Zanini, M.; Shirvani, H.; Cheng, J.-S.; Yu, H.; Feng, C.-H.; Mercier, A.L.; Hung, S.-Y.; Forget, A.; Wang, C.-H.; et al. Atoh1 Controls Primary Cilia Formation to Allow for SHH-Triggered Granule Neuron Progenitor Proliferation. *Developmental Cell* **2019**, *48*, 184-199.e5, doi:10.1016/j.devcel.2018.12.017.
53. Berbari, N.F.; Bishop, G.A.; Askwith, C.C.; Lewis, J.S.; Mykytyn, K. Hippocampal Neurons Possess Primary Cilia in Culture. *J. Neurosci. Res.* **2007**, *85*, 1095–1100, doi:10.1002/jnr.21209.
54. Kalil, K.; Dent, E.W. Branch Management: Mechanisms of Axon Branching in the Developing Vertebrate CNS. *Nat Rev Neurosci* **2014**, *15*, 7–18, doi:10.1038/nrn3650.
55. Miller, K.E.; Suter, D.M. An Integrated Cytoskeletal Model of Neurite Outgrowth. *Front. Cell. Neurosci.* **2018**, *12*, 447, doi:10.3389/fncel.2018.00447.
56. Armijo-Weingart, L.; Gallo, G. It Takes a Village to Raise a Branch: Cellular Mechanisms of the Initiation of Axon Collateral Branches. *Molecular and Cellular Neuroscience* **2017**, *84*, 36–47, doi:10.1016/j.mcn.2017.03.007.
57. Pinskey, J.M.; Franks, N.E.; McMellen, A.N.; Giger, R.J.; Allen, B.L. Neuropilin-1 Promotes Hedgehog Signaling through a Novel Cytoplasmic Motif. *Journal of Biological Chemistry* **2017**, *292*, 15192–15204, doi:10.1074/jbc.M117.783845.
58. Choksi, S.P.; Lauter, G.; Swoboda, P.; Roy, S. Switching on Cilia: Transcriptional Networks Regulating Ciliogenesis. *Development* **2014**, *141*, 1427–1441, doi:10.1242/dev.074666.
59. Thomas, J.; Morlé, L.; Soulavie, F.; Laurençon, A.; Sagnol, S.; Durand, B. Transcriptional Control of Genes Involved in Ciliogenesis: A First Step in Making Cilia. *Biology of the Cell* **2010**, *102*, 499–513, doi:10.1042/BC20100035.
60. Andermatt, I.; Wilson, N.; Stoeckli, E.T. In Ovo Electroporation of miRNA-Based-Plasmids to Investigate Gene Function in the Developing Neural Tube. In *Gene Function Analysis*; Ochs, M.F., Ed.; Methods in Molecular Biology; Humana Press: Totowa, NJ, 2014; Vol. 1101, pp. 353–368 ISBN 978-1-62703-720-4.
61. Wilson, N.H.; Stoeckli, E.T. Cell Type Specific, Traceable Gene Silencing for Functional Gene Analysis during Vertebrate Neural Development. *Nucleic Acids Research* **2011**, *39*, e133–e133, doi:10.1093/nar/gkr628.
62. Williams, R.M.; Senanayake, U.; Artibani, M.; Taylor, G.; Wells, D.; Ahmed, A.A.; Sauka-Spengler, T. Genome and Epigenome Engineering CRISPR Toolkit for *in Vivo* Modulation of *Cis* -Regulatory Interactions and Gene Expression in the Chicken Embryo. *Development* **2018**, *145*, dev160333, doi:10.1242/dev.160333.
63. Gandhi, S.; Piacentino, M.L.; Vieceli, F.M.; Bronner, M.E. Optimization of CRISPR/Cas9 Genome Editing for Loss-of-Function in the Early Chick Embryo. *Developmental Biology* **2017**, *432*, 86–97, doi:10.1016/j.ydbio.2017.08.036.
64. Hamburger, V.; Hamilton, H.L. A Series of Normal Stages in the Development of the Chick Embryo. *J. Morphol.* **1951**, *88*, 49–92, doi:10.1002/jmor.1050880104.
65. Andermatt, I.; Wilson, N.H.; Bergmann, T.; Mauti, O.; Gesemann, M.; Sockanathan, S.; Stoeckli, E.T. Semaphorin 6B Acts as a Receptor in Post-Crossing Commissural Axon Guidance. *Development* **2014**, *141*, 3709–3720, doi:10.1242/dev.112185.
66. Wilson, N.H.; Stoeckli, E.T. In Ovo Electroporation of MiRNA-Based Plasmids in the Developing Neural Tube and Assessment of Phenotypes by DiI Injection in Open-Book Preparations. *JoVE* **2012**, 4384, doi:10.3791/4384.
67. Das, R.M.; Storey, K.G. Apical Abscission Alters Cell Polarity and Dismantles the Primary Cilium During Neurogenesis. *Science* **2014**, *343*, 200–204, doi:10.1126/science.1247521.

68. Dumoulin, A.; Dagane, A.; Dittmar, G.; Rathjen, F.G. S-Palmitoylation Is Required for the Control of Growth Cone Morphology of DRG Neurons by CNP-Induced CGMP Signaling. *Front. Mol. Neurosci.* **2018**, *11*, 345, doi:10.3389/fnmol.2018.00345.
69. Schindelin, J.; Arganda-Carreras, I.; Frise, E.; Kaynig, V.; Longair, M.; Pietzsch, T.; Preibisch, S.; Rueden, C.; Saalfeld, S.; Schmid, B.; et al. Fiji: An Open-Source Platform for Biological-Image Analysis. *Nat Methods* **2012**, *9*, 676–682, doi:10.1038/nmeth.2019.